CHEMISTRY
A European Journal

A Journal of
ChemPubSoc Europe

Accepted Article

Title: Role of Halide Ions on the Nature of Magnetic Anisotropy in Tetrahedral Co(II) Complexes

Authors: Maheswaran Shanmugam, Shefali Vaidya, Saurabh Kumar Singh, Pragya Shukla, Kamaluddin Ansari, and Gopalan Rajaraman

To be cited as: *Chem. Eur. J.* 10.1002/chem.201606031

Link to VoR: http://dx.doi.org/10.1002/chem.201606031

Supported by
ACES

WILEY-VCH

10.1002/chem.201606031

WILEY-VCH

Role of Halide Ions on the Nature of Magnetic Anisotropy in Tetrahedral Co(II) Complexes

Shefali Vaidya,[a] Saurabh Kumar Singh,[a],[b] Pragya Shukla,[a] Kamaluddin Ansari,[a] Gopalan Rajaraman*[a] and Maheswaran Shanmugam*[a]

Abstract: A series of mononuclear tetrahedral Co(II) complexes with a general molecular formula of $[CoL_2X_2]$ (where L= thiourea and X = Cl (**1**), Br (**2**) and I (**3**)) were synthesized and their structures were characterized by single crystal x-ray diffraction. Detailed direct current (dc) magnetic susceptibility ($\chi_M T(T)$ and $M(H)$) and its slow relaxation of magnetization measurements were performed on all the three complexes. The experimental dc magnetic data is excellently reproduced by fitting both $\chi_M T(T)$ and $M(H)$ simultaneously using the parameters D = +10.8 cm^{-1}, g_1 = 2.2, g_2 = 2.2, and g_3 = 2.4 for **1**; D = -18.7 cm^{-1}, g_{iso} = 2.21 for **2**; D = -19.3 cm^{-1}, g_{iso} = 2.3 for **3**. The replacement of chloride anion in **1** by bromide or iodide (in **2** and **3** respectively) accompanied by not only change in sign of magnetic anisotropy (D), but also in magnitude. Field induced out-of-phase susceptibility signals are observed in 10% diluted sample of **1**-**3** implies the slow relaxation of magnetization behavior of molecular origin. To better understand the magnetization relaxation dynamics of complexes **1**-**3** detailed ab initio CASSCF/NEVPT2 calculations were performed. The computed spin Hamiltonian parameters are in good agreement with experimental data. Particularly calculations unveil the role of halogen atom in switching the sign of D as we move from $–Cl^-$ to $–I^-$. Large spin-orbit coupling constant associated with the heavier halide ion and weaker π donation reduces the ground state-excited state gap leads to larger contribution to negative D for the complex **3** compared to complex **1**. Further magneto-structural D correlations are developed to understand the role of structural distortion on the sign and magnitude of D values in this family of complexes.

Introduction

Slow relaxation of magnetization arises in certain oligomeric complexes due to the presence of easy or Ising type magnetic anisotropy associated with the overall ground state of a molecule. Such phenomenon is termed as Single-molecule-magnets (SMM), if the phenomenon originates due to a single metal ion or monomeric coordination complexes it is known as single-ion magnets (SIM). Such SMM property was first discovered in {Mn12OAc} complex.[1] After the discovery, numerous transition metal complexes[2] were flooded in the literature with a record breaking ground state (83/2 for a Mn19 cluster) reported by Powell and co-workers[3] and an effective energy barrier (U_{eff}, 86 K for Mn6 cluster) for the magnetization relaxation by Brechin and co-workers[4] independently, as SMM can be envisaged for many potential applications such as high density storage, spin valves, spintronic, Quantum computing etc.[5] Over the period of three decades, it has been realized that due to the random easy axis orientations in larger cluster, overall magnetic anisotropy (D) becomes small, although complexes were stabilized with relatively large ground state. Ideally, there are no parameters available to enhance the D and S simultaneously in oligomeric complexes which is also evident that D is approximately equals to $1/S^2$ of the complex.[6] Due to this persistent problem researchers focused their attention to modulate the D value of the mononuclear transition metal complexes. The majority of the transition metal complexes suffer with low spin-orbit coupling as the orbital angular momentum is reduced by the ligand field. Restricting the coordination number around the transition metal is found to be a fruitful way to gain orbital angular momentum[7] and such synthetic strategy was proven successful in a two coordinate Co(II) and Fe(I) complex with the largest anisotropic barrier 578.2 K and 225 K respectively reported to date for any transition metal SMMs by Gao and Co-workers and Long and co-workers independently.[8] In addition, several other approaches have been reported in the literature to gain orbital angular momentum, to maximize the magnetic anisotropy in mononuclear complexes. For examples, the substituent on the ligand modulate U_{eff} (by means of D),[2e, 9] in-plane and out-of plane shift of metal ion in a five coordinate Co(II) complexes[10], by changing the halides in an octahedral and certain tetrahedral complexes,[11] structural distortion around metal centers and even more intricate factors such as secondary coordination sphere has a significant effect on modulating D-value which was elegantly explained by Neese and co-workers theoretically and experimentally proven by us recently.[12] To modulate the sign of magnetic anisotropy, we have proposed a novel synthetic strategy recently i.e. employing a soft donor ligand (such as sulfur) stabilizes easy axis anisotropy, while the hard donor favours easy plane magnetization orientation.[13]

In this line of interest, we intend to probe the influence of other commonly known ligand such as halides in controlling the spin Hamiltonian parameters of the complexes, apart from the soft donor “L” ligand. For this purpose, we have synthesized a series of monomeric Co(II) tetrahedral thiourea complexes and their magnetic properties were investigated in details. The observed change in Spin Hamiltonian (SH) parameters and its slow magnetization relaxation behavior of these complexes were rationalized by detailed theoretical calculations.

Results and Discussion

Recently we and others have pointed out that by employing soft donor ligand such as sulfur in a tetrahedral Co(II) environment,

[a] S. Vaidya, Dr. S.K. Singh, P. Shukla, K. Ansari, Prof. G. Rajaraman and Prof. M. Shanmugam
Department of Chemistry, Indian Institute of Technology Bombay
Powai, Mumbai-400076, Maharashtra, India.
E-mail: rajaraman@chem.iitb.ac.in, eswar@chem.iitb.ac.in
[b] Dr. S. K. Singh
Department of Molecular Theory and Spectroscopy, Max-Planck Institute for Chemical Energy Conversion, Mülheim an der Ruhr, D-45470, Germany

stabilize easy axis magnetic anisotropy.[13-14] This proposed idea has been proven by us recently by employing a totally different soft donor (thiourea and its derivatives) ligands.[12c] In order to probe the influence of the other ligated atoms such as halides apart from the soft donor ligands, we have synthesized a series of monomeric Co(II) complexes. When one equivalent of alcoholic solution of $CoX_2.xH_2O$ (where X = Cl or Br or I) is treated with two equivalent of thiourea, yields blue color single crystal which are suitable for single crystal x-ray diffraction. The structure solution and refinement reveals the molecular formulae of all the three complexes as $[CoX_2L_2]$ where L = thiourea ($(NH_2)_2CS$); X = Cl (**1**) or Br (**2**) or I (**3**) (Figure 1). The complexes **1**-**3** were crystallized in a monoclinic *Cc* (for **1**) and $P2_1/c$ (for **2** and **3**) space group. The crystallographic parameters for all the three complexes are given in Table 1.

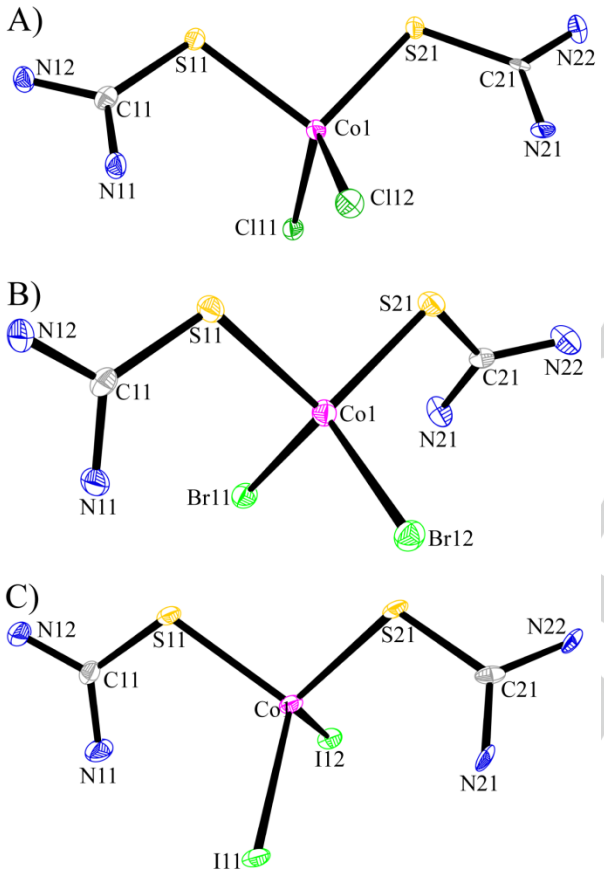

Figure 1. Thermal ellipsoid (50% probability) representation of complexes A) **1** B) **2** C) **3**.

In all the three complexes the divalent cobalt ion exists in a distorted tetrahedral geometry. Two out of four coordination sites are occupied by thiourea ligand while the other two sites are completed by two halide ions in respective complexes. The average Co-S bond distance found to be 2.302(10) Å, 2.307(9) Å, 2.319(10) Å for complexes **1**-**3** respectively. While the average bond length for Co-X (where X = Cl or Br or I; 2.258(9) Å for **1**; 2.401(5) Å for **2**; 2.602(5) Å for **3**) increases upon increasing the atomic radii of the halide ion in complex. But the extent of increase in bond lengths of Co-X in all the three complexes is larger than the Co-S bond length. The bond angle of ∠X11-Co1-X12 in all the three complexes are close to the tetrahedral angle ie. 107.82°(3), 108.40°(3) and 107.25°(2) for **1**-**3** respectively. However, drastic change is noticed with the bond angle of ∠S11-Co-S12 96.63°(3) (for **1**), 101.43°(3) (for **2**), and 100.32°(4) (for **3**). Selected bond lengths and bond angles of complexes **1**-**3** are given in Table 2. Detailed structural analysis of all the three complexes reveal that there is hydrogen bonding network across all the directions. In complexes **1**-**3**, the protons on the amino group of thiourea ligand are involved in hydrogen bonding with halide ions as well as the sulfur atom. Apart from the intermolecular hydrogen bonding, intramolecular hydrogen bonding also exists in the crystal structure. The atoms involved in both intra and intermolecular hydrogen bonding are listed in Tables S1-S3 for all the three complexes.

Table 1. Crystallographic data for complexes **1**-**3**.

	1	**2**	**3**
Formula	$CoC_2H_8Cl_2N_4S_2$	$CoC_2H_8Br_2N_4S_2$	$CoC_2H_8I_2N_4S_2$
Size (mm)	0.20 x 0.16 x 0.11	0.35 x 0.17 x 0.08	0.58 x 0.22 x 0.12
System	Monoclinic	Monoclinic	Monoclinic
Space grp.	*Cc*	$P2_1/c$	$P2_1/c$
a [Å]	8.1970(16)	10.163(4)	10.483(3)
b [Å]	11.528(2)	6.977(2)	7.3377(17)
c [Å]	10.794(2)	14.562(5)	14.813(4)
α [°]	90.0000	90.0000	90.0000
β [°]	103.56(3)	93.207(5)	91.344(3)
γ [°]	90.0000	90.0000	90.0000
V [Å^3]	991.5(3)	1030.9(6)	1139.1(5)
Z	4	4	4
ρ_{calcd}[g/cm^{-3}]	1.890	2.390	2.711
$2\Theta_{max}$	58.28	58.3	58.34
radiation	Mo K_α	Mo K_α	Mo K_α
λ [Å]	0.71073	0.71073	0.71073
T [K]	100	100	100
reflns	5985	19068	14607
Ind. reflns	2585	2770	3046
reflns with *I*>2σ(*I*)	2310	2065	2251
R1	0.0242	0.0304	0.0275
wR2	0.0683	0.0478	0.0597

The packing diagram of **1** is distinctly different from complex **2** or **3** (Figure 2A). Since complexes **2** and **3** possess a similar packing arrangement, a representative packing diagram is shown in Figure 2B. In complex **1**, hydrogen bonding exists between N-H….S11 (2.624(3) Å) is relatively stronger than N-H….Cl (3.093(2) Å).

Table 2. Selected bond lengths and bond angles parameter for complexes **1**-**3**.

Label	**1** (Å)	**2** (Å)	**3** (Å)
Co1-S11	2.297(10)	2.303(9)	2.308(10)
Co1-S21	2.307(10)	2.311(9)	2.330(11)
Co1-X11	2.249(9)	2.397(6)	2.595(6)
Co1-X12	2.268(9)	2.405(5)	2.608(5)
	Bond angle (°)		
X11-Co1-X12	107.82(3)	108.40(3)	107.25(2)
X11-Co1-S11	116.02(4)	111.65(3)	111.86(3)
X12-Co1-S11	106.96(4)	109.87(3)	116.73(3)
X11-Co1-S21	113.46(4)	110.05(3)	110.45(3)
X12-Co1-S21	115.72(4)	115.36(3)	110.07(3)
S11-Co1-S21	96.63(3)	101.43(3)	100.32(4)

Variation in the H-bonding strength in **1** is likely due to the short Co(II)….Co(II) distance found between two molecules (see Figure 2 for details). Such supramolecular interaction is likely to play a significant role in magnetization relaxation dynamics. From the packing diagram of complex **1**, it is clearly witnessed that a layer of molecules along the c-axis are orienting in the same direction, while the adjacent layer is generated by c-glide. Although the interatomic distance of Co(II)….Co(II) found in **2** (5.853(3)) and **3** (5.932(2) Å) is shorter than distance found in **1**, the H-bonding strength observed in complex **2** and **3** is weaker than in **1** (see Tables S1-S3 and figure S1 for details).

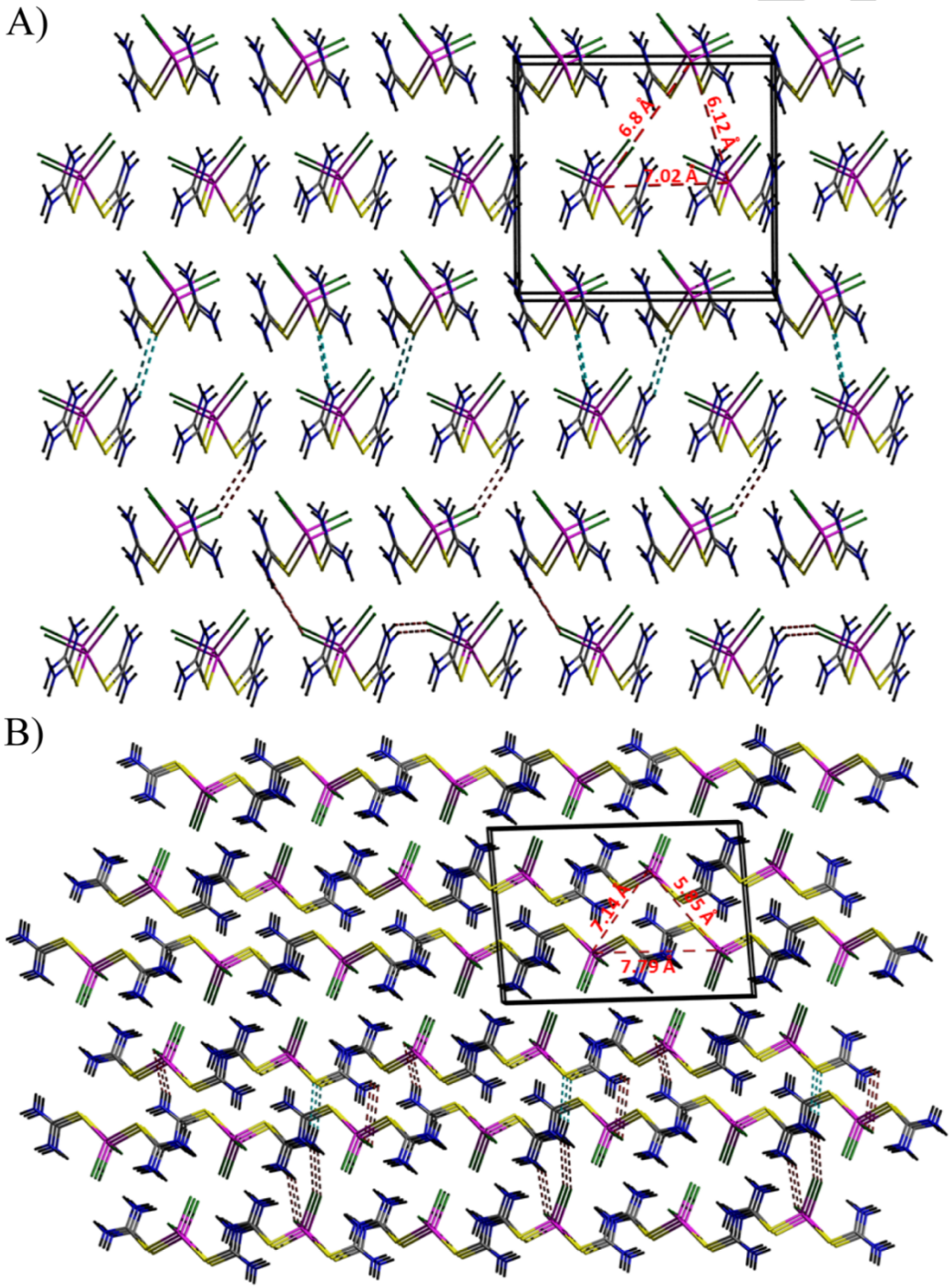

Figure 2. Packing diagram of complex **1** (panel A) and complex **2** (panel B). Sky blue dotted bonds represent intermolecular H-bonding between sulfur and proton (-NH_2) and wine red dotted bond denotes H-bonding between halide and proton (-NH_2) in the crystal lattice. Colour code: Magenta = Co(II), green = X (X = Cl (for **1**) or Br (for **2**)), blue = N, yellow = S.

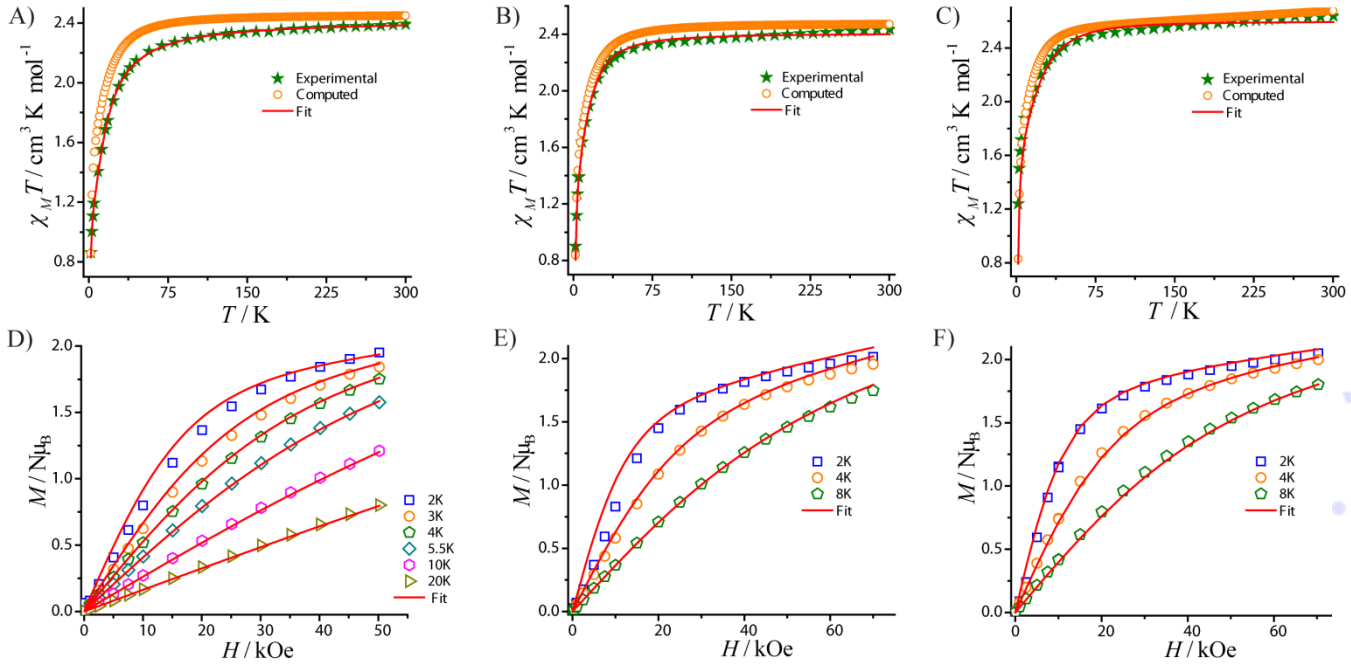

Figure 3. Panels A-C) Direct current magnetic susceptibility measurement performed on polycrystalline sample of complexes **1**-**3** respectively in the presence of an external magnetic field of 1 kOe. The open circle in those panel represents the simulation of the experimental magnetic data using the SH parameters computed from CASSCF / NEVPT2 calculations described in main text. Panels D-F) Field dependent magnetization measurements were performed at the indicated temperatures. The solid red line in all the panels represents the simultaneous magnetic data ($\chi_M T$(*T*) and *M*(*H*)) fitting using the parameters described in Table 3 (*vide infra*).

Direct current (dc) magnetic susceptibility data of complexes 1-3.

Variable temperature direct current magnetic susceptibility measurements were performed on polycrystalline samples of all the three complexes in the temperature range of 2.0 - 300 K in the presence of an external magnetic field of 1 kOe (Figure 3). The room temperature (RT) $\chi_M T$ value for all the three complexes **1** – **3** are 2.40, 2.52, 2.63 cm^3 K mol^{-1} respectively which are significantly higher than the expected value for a mononuclear Co(II) (S = 3/2) ion with no first order orbital angular momentum (1.875 cm^3Kmol^{-1}, g = 2). The temperature dependent $\chi_M T(T)$ behavior of all the three complexes is almost similar, i.e. a gradual decrease in $\chi_M T$ value is noticed upon lowering the temperature from room temperature (RT) to 50 K. The observed temperature dependency in this temperature region (RT to 50 K) for a mononuclear Co(II) complex designates the depopulation of the Kramers-state. There is a sharp decrease in $\chi_M T$ value below 50 K and reaches a value of 0.861, 0.900, 1.240 cm^3 K mol^{-1} at 2.0 K for complexes **1**-**3** respectively. Several factors such as I) magnetic anisotropy associated with the complex II) intermolecular antiferromagnetic interaction III) dipolar interactions are likely to contribute to the sharp decrease in $\chi_M T$ value at low temperature.

Field dependent magnetization measurements were performed at various temperatures (2-10 K) for complexes **1**-**3** up to 70 kOe. The magnetic moment gradually increases upon increasing the external magnetic field and the magnetic moment tend to saturate around 1.95, 2.01, and 2.04 $N\mu_B$ at 2.0 K for complexes **1**-**3** respectively (Figure 3). The observed magnetic moment at this temperature is significantly lower than the expected value indicates the presence of magnetic anisotropy associated with the ground state in all the complexes. The non-superimposable nature of the reduced magnetization curve of all the three complexes further supports the presence of magnetic anisotropy (Figure S2). In order to extract the spin Hamiltonian (SH) parameters of all the three complexes, we have fitted the magnetic data of both $\chi_M T(T)$ and *M*(*H*) simultaneously using PHI software.[15] The Hamiltonian used for fitting the data is given below.

$$H = D\left\{S_z^2 - \frac{S(S+1)}{3}\right\} + E\left(S_x^2 - S_y^2\right) + g\mu_B H.S \qquad (1)$$

In order to reduce the over parameterization, we have fitted the magnetic data using isotropic g-value for all the complexes except for complex **1** and the obtained parameters are listed in Table 3. An excellent agreement between the fit and the experimental magnetic data obtained using the parameters *D* = +10.8 cm^{-1} (g_{xx} = 2.2, g_{yy} = 2.2, g_{zz} = 2.4; |E/D| = 0.11, for **1.** While the simultaneous $\chi_M T(T)$ and *M*(*H*) data fit of **2** and **3** yields the *D*-value of -18.7 cm^{-1} (g_{iso} = 2.21) and -19.3 cm^{-1} (g_{iso} = 2.3) respectively (Table 3). Here we would like to point out that, the experimental $\chi_M T(T)$ fit alone is insensitive to the sign of *D*-value i.e. either with positive *D* or negative *D*, experimental $\chi_M T(T)$ data could be modeled. However, the parameters extracted while incorporating negative *D* for **1** results in unreliable SH parameters (data not shown) while positive *D* for **2**

and **3** respectively did yield poor fit for *M*(*H*) data for these complexes (see Table S4 and Figure S3 of ESI). This evidently suggest that simultaneous fit of magnetic data ($\chi_M T(T)$ and *M*(*H*)) facilitate to reliably extract the sign and magnitude of *D* value for all the complexes (Table 3). Such an approach is fruitful for unambiguous determination of sign of *D* using dc magnetic data for majority of the complexes reported in the literature.[13a, 16]

Table 3. Spin Hamiltonian parameters extracted from CASSCF / NEVPT2[a] calculations and PHI[b] fitting[15] for the complexes **1**-**3**.

	D_{cal}[a] (cm^{-1})	D_{fit}[b] (cm^{-1})	|E/D| Cal	|E/D| fit	g_{xx}, g_{yy}, g_{zz}[a]	g_{xx}, g_{yy}, g_{zz}[b]
1.	17.4	+10.8	0.25	0.11	2.16,2.30,2.41	2.2, 2.2, 2.4
2.	±14.9	-18.7	0.32	-	2.18,2.29,2.42	2.21 (g_{iso})
3.	-18.3	-19.3	0.25	-	2.19,2.29,2.46	2.3 (g_{iso})

The observation of positive *D*-value for **1** is quite different from our earlier prediction[13a] and we also notice that there is a drastic change in magnitude of magnetic anisotropy in all the complexes compared to the series of $[CoS_4]^{2-}$ complexes reported by us recently.[12c] The notable changes observed in the Spin Hamiltonian parameters of complexes **1**-**3** are rationalized by detailed computational calculations (*vide infra*).

Electron paramagnetic resonance (EPR) measurements of complexes 1-3.

To support the parameters extracted from the magnetic data fit, we have recorded X-band EPR spectra of complexes **1** - **3** at 5 K both in both solid (100% and diluted sample) and frozen solutions. Complex **1** was EPR silent above 100 K both in solid and frozen solution spectra recorded, while complexes **2** and **3** show a broad EPR signals at 100 K (see Figures S4-S6). This is probably due to the intricate electronic structure associated with ^{59}Co(II) ion possessing an hyperfine of I=7/2 and its associated fast relaxation phenomenon. Further, we would like to point out that accurate determination of zero field splitting (ZFS) is extremely difficult using low frequency EPR spectroscopy as its microwave quanta is considerably smaller than the ZFS observed in complexes **1**-**3**. At 5.0 K, EPR spectral features of 100% polycrystalline sample of **1** are distinctly different from complexes **2** and **3** suggest that the electronic structure associated with these complexes must be different, while complexes **2** and **3** show similar EPR spectral features (see Figure 4). It is very well witnessed in the literature that a high spin Co(II) complex stabilized with easy axis anisotropy is expected to be EPR silent at 5.0 K under strictly axial condition due to the forbidden $\Delta Ms = \pm 3$ intra Kramers transition.[11h, 17] However, for **2** and **3**, broad EPR transitions arising from ground Kramers doublet observed around 3500 G and 9000 G is due to non-zero rhombicity (E/D = 0.32 (for **2**) and 0.25 (for **3**)) associated with these complexes, which mixes the pure wave functions of two Kramers doublet. Similar EPR spectral features (broad EPR signals around 3500 G and 9000 G) were observed in frozen solution and magnetically diluted samples of **2** and **3** (see Figures S5-S6). Such scenario have been witnessed in many high spin Co(II) complexes stabilized with easy axis anisotropy. [11h, 17]

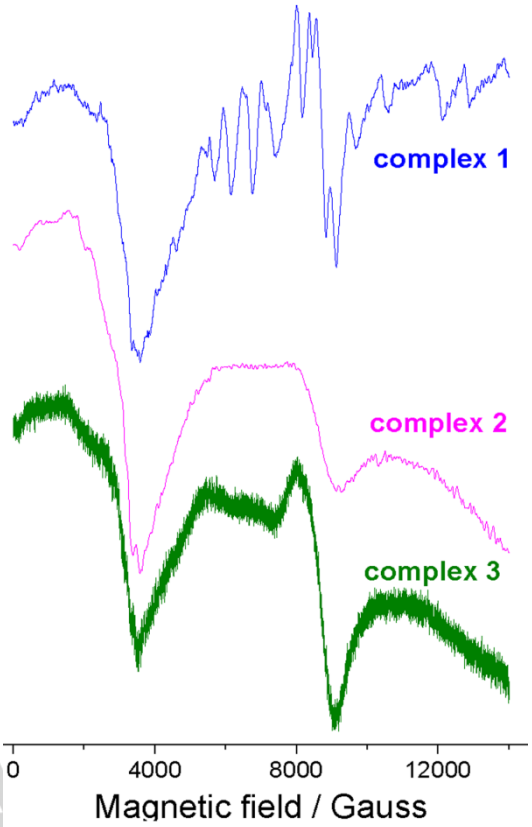

Figure 4. X-band EPR spectra of frozen ethanol-toluene solution of complexes **1**-**3** recorded at 5 K. Condition: microwave power = 10 dB (**1**), 18 dB(**2**), 20 dB(**3**) (20 mW (**1**), 3.17 mW (**2**), 2mW (**3**)), modulation amplitude = 0.4 mT (**1**), 1.45 mT (**2**), 0.4 mT, microwave frequency = 9.37 GHz, Temp = 5K,

In contrast to complexes **2** and **3**, both frozen solution and 2% diluted sample of **1** shows well resolved peaks indicative of the signal arising from ±1/2 ground Kramers state ($\Delta M_s = \pm 1$) (see Figure S4). Variable temperature EPR spectra recorded on frozen solution spectra evidently shows that the intensity of the all the signal decreases upon increasing the temperature. Since the entire EPR spectral features of complex **1** are not feasible with low frequency EPR instrument, we have not attempted to do EPR simulation for **1**, which might lead to estimation of unreliable spin Hamiltonian parameters.

Although EPR experiments performed does not facilitate to quantify the magnitude of *D* accurately, it gives strong experimental evidence for the sign of magnetic anisotropy extracted from the magnetic data fit of complexes **1**-**3**, ie. complex **1** stabilized with easy plane anisotropy while **2** and **3** possess easy axes anisotropy. This is further strongly corroborated by *ab initio* calculations (*vide infra*).

Alternating current (ac) magnetic susceptibility data of complexes 1-3.

To probe the magnetization relaxation dynamics of all the three complexes, ac susceptibility measurements were performed on polycrystalline sample of **1**-**3** with 3.5 Oe ac oscillating field with and without the external bias field between 1.8 and 8.0 K. For complex **1**, no frequency dependent out-of-phase susceptibility signals (χ_M'') were observed under a zero applied field. This is not surprising for a complex (**1**) that possesses easy plane

magnetic anisotropy. However, ac data were collected in the presence of 2 kOe dc bias field, we do observe χ_M" signals indicative of field induced slow relaxation of magnetization shown in Figure 5.

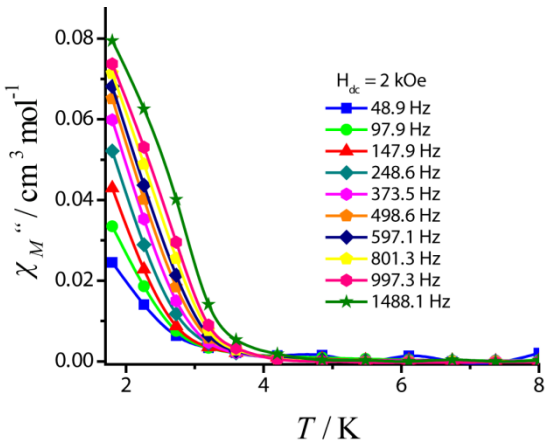

Figure 5. Frequency dependent out-of-phase (χ_M") susceptibility signal observed for 100% sample of complex **1** in the presence of external magnetic field of 2 KOe at the indicated frequency.

Similar behavior has been observed for the majority of tetrahedral complexes stabilized with positive anisotropy in the literature.[18] Ruiz and co-workers elegantly explain the rationale for the slow relaxation of magnetization in a molecule with positive D value.[19] Although complex **1** shows χ_M" signals, the maxima are observed well below the instrument limit which hampers to extract the barrier for the magnetization relaxation. To our surprise, although complexes **2** and **3** possess negative anisotropy, there are no frequency dependent out-of-phase susceptibility signals observed in ac measurement, both in the presence and absence of an external magnetic field. The absence of χ_M" even in the presence of dc bias field suggests that quantum tunneling of magnetization is extremely fast over the thermal relaxation mechanism (Orbach Process). Further, the magnetization relaxation can be triggered by the nuclear hyperfine interaction of Co(II) and the coordinated halide ions, in addition to the supramolecular interaction mediated through the hydrogen bonding.

As pointed out earlier, in all the complexes (**1**-**3**) both intra and intermolecular hydrogen bonding spread across all direction. Often such supramolecular interaction leads to faster magnetization relaxation or the observed slow relaxation phenomenon could be due to magnetic ordering. In order to understand the role of dipolar interaction and to identify the slow relaxation magnetization behavior is single molecular origin or not, we have performed ac relaxation dynamics studies on the magnetically diluted sample of all the complexes (see experimental section for details). In all the diluted samples, we do observe frequency dependent out-of-phase susceptibility signals in the presence of optimum external magnetic field suggests that the slow relaxation of magnetization behavior in the complexes **1**-**3** is of single-molecule origin rather magnetic ordering phenomenon.

To gain more insight into the magnetization relaxation phenomenon, the ac data of all the complexes were analyzed in details. The frequency dependent out-of-phase susceptibility data of diluted complex **1** is shown in Figure 6 carried out at an optimum field of 5.5 kOe (see Figure S7).

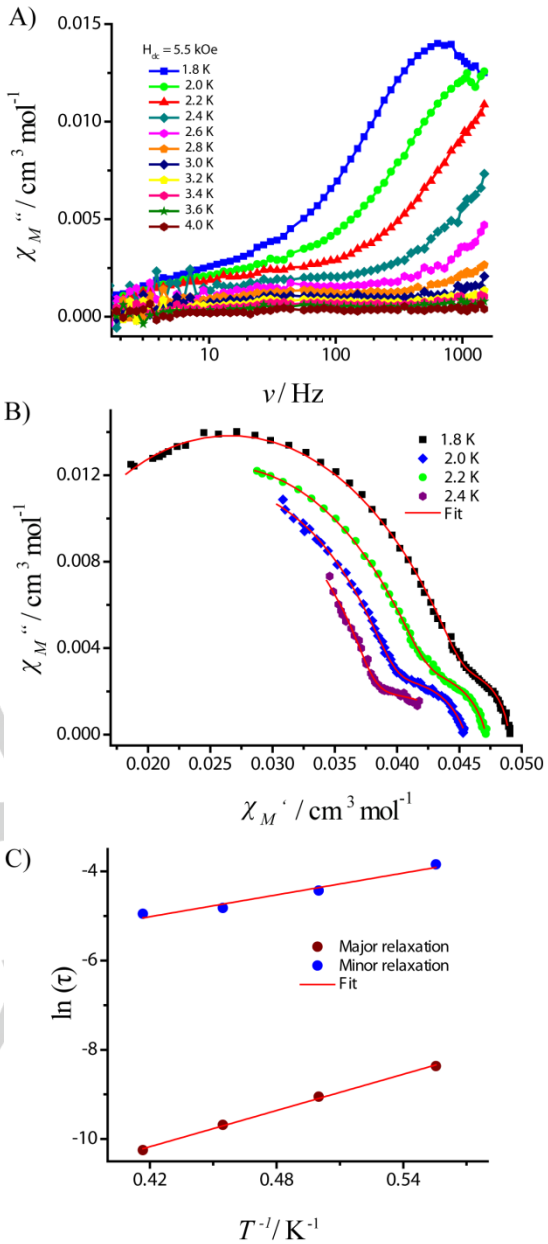

Figure 6. Ac measurement for 10% diluted sample of complex **1**. A) Frequency dependent dependent out-of-phase susceptibility signals at the indicated optimum dc magnetic field B) Cole-Cole plot at the indicated temperatures C) Arrhenius plot of complex **1**. The solid red line represents the fit of the data.

From figure 6A (also see Figure S8A) it is evident that there are two kinds of relaxation i.e. majority of the fraction undergo faster relaxation and a non-negligible fraction follows a slow relaxation process. The fast relaxation (major relaxation) and slow relaxation phenomenon observed in **1** is very well witnessed in Cole-Cole plot of the complex, particularly at lower temperature (see Figure 6C). The Cole-Cole plot of **1** was fitted considering two relaxation processes using generalized Debye model (equation 2) given below.

$$\chi_{AC}(\omega) = \chi_{S,tot} + \frac{\Delta\chi_1}{1+(i\omega\tau_1)^{(1-\alpha_1)}} + \frac{\Delta\chi_2}{1+(i\omega\tau_2)^{(1-\alpha_2)}} \dots (2)$$

The α_1 values ranges from 0.21 to 0.06 and α_2 ranges from 0.07 to 0.6 between 1.8 K – 2.4 K temperature ranges (see Table S5). The relaxation time extracted (τ_1 and τ_2) from Cole-Cole fitting is employed to construct the Arrhenius plot (Figure 6C). The linear fit of this data considering only the Orbach process results in the effective energy barrier of 13.5 K (τ_0 = 1.37 x 10^{-7} s) and 8.15 K (τ_0 = 2.2 x 10^{-4} s).

On the contrary to **1** (diluted sample), complex **2** (10% diluted sample) indeed shows a well resolved frequency dependent χ_M" signals in the presence of optimum external magnetic field of 2 kOe (Figure 7 and Figure S7). The presence one single major relaxation is firmly corroborated by the Cole-Cole plot of **2** (Figure 7B and Figure S8B). The Cole-Cole plot was fitted by considering a single relaxation process using the generalized Debye equation (equation 3) and the extracted parameters are shown in Table S6.

$$\chi_{AC}(\omega) = \chi_S + \frac{\chi_T - \chi_S}{1 + (\iota\omega\tau)^{(1-\alpha)}} \quad (3)$$

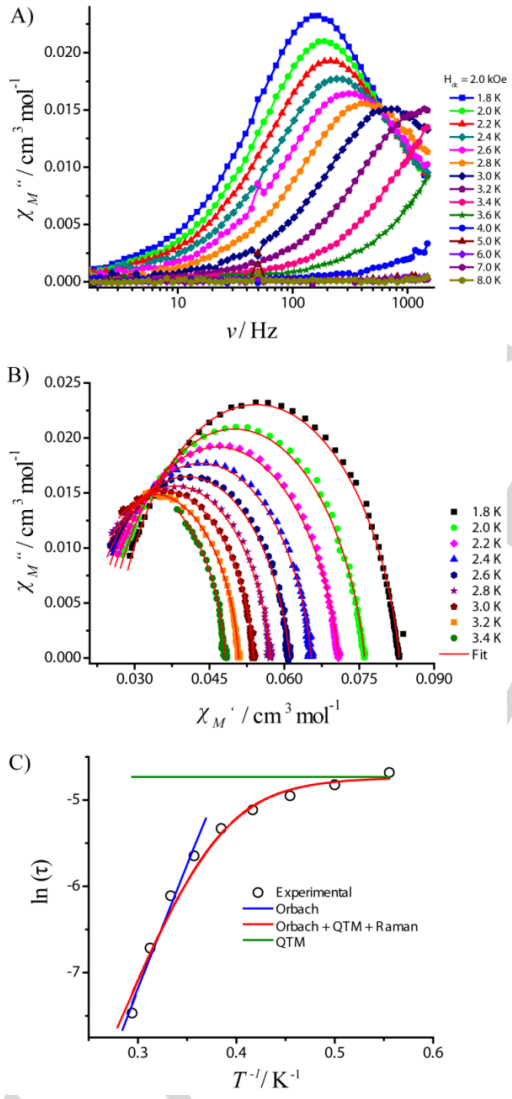

Figure 7. Ac measurement for 10% diluted sample of complex **2**. A) Frequency dependent out-of-phase susceptibility signals at the indicated optimum dc magnetic field B) Cole-Cole plot at the indicated temperatures C) Arrhenius plot of complex **2**. The solid red line represents the fit of the data.

The α values are ranging between 0.09 and 0.15 in the temperature range of 3.6 K to 1.8 K. This suggests the presence of narrow distribution of relaxation times. Using the τ values obtained from the Cole-Cole fit, we have constructed the Arrhenius plot (Figure 7C). Below 3.5 K, apart from Orbach process, other relaxation processes (such as direct, QTM and Raman processes) appears to be operative. The data was fitted according to equation 4, which takes into account of various relaxation processes.

$$\frac{1}{\tau} = \frac{1}{\tau_{QTM}} + AH^2T + CT^n + \frac{1}{\tau_0}\exp\left(\frac{-U_{eff}}{k_BT}\right) \quad (4)$$

Where $\mathbf{1}/\boldsymbol{\tau_{QTM}}$ represents relaxation via QTM, $\boldsymbol{AH^2T}$ represents direct process, $\boldsymbol{CT^n}$ is for Raman process and the last terms describes the relaxation via Orbach process.

It is not necessary to use all the relaxation process to fit the Arrhenius plot of **2**. By considering only Orbach (28.6 K (τ_0 = 1.66 x 10^{-7} s)), QTM (0.0088 s) and Raman (C = 0.065 $s^{-1}K^{-3}$ and n = 6), excellent fit to the experimental data obtained.

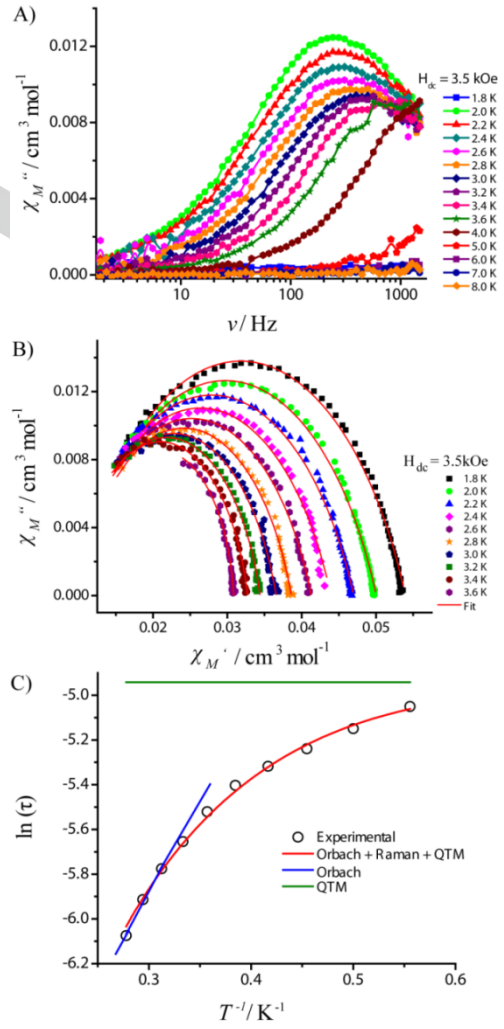

Figure 8. Ac measurement for 10% diluted sample of complex **3**. A) Frequency dependent dependent out-of-phase susceptibility signals at the indicated optimum dc magnetic field B) Cole-Cole plot at the indicated temperatures C) Arrhenius plot of complex **3**. The solid red line represents the fit of the data.

In line with the magnetization relaxation behavior of **2**, complex **3** (10% diluted sample) also exhibit a similar relaxation behavior (Figure 8), however, slightly higher dc-bias field (H_{dc} = 5.5 kOe, Figure S7) is required to observe the frequency dependent out-of-phase susceptibility signals in **3** compared to **2** (H_{dc} = 2 kOe). The τ value extracted from Cole-Cole fit data employed to construct the Arrhenius plot. The experimental data were fitted considering multiple relaxations (equation 4). Reasonably good fit were obtained by taking into account of only Orbach (9 K, τ_0 = 4.06 x 10^{-4} s), Raman (C = 0.034 $s^{-1}K^{-3}$ and n = 6 value) and QTM (0.007 s) processes (see Figure 8C).

To fully understand the magnetization relaxation dynamics observed in all the three complexes, trend found in the estimated magnetic anisotropy and to unequivocally establish the role of halide ions in modulating the *D* and *E* values, ab initio calculations were performed on complexes **1**-**3.**

Computational studies of complexes 1-3.

CASSCF and NEVPT2 calculations have been performed on complexes **1**-**3** to understand the reason behind the origin of positive (for **1**) and negative (for **2** and **3**) zero field splitting (zfs) parameters in these complexes (see computational details). We have also attempted to shed light on the role of structural distortions on the magnetic anisotropy of these complexes. The computed Spin-Hamiltonian (SH) parameters (*D*, *E* and g values) for all the three complexes are listed in Table 3. The simulation of experimental magnetic susceptibility data using the computed SH parameters is in good agreement (see Figure 3), which reflects the reliability of the computed parameters. It is evident from table 3 that for all the three complexes, ab initio calculated |E/D| values are quite large. Particularly for complex **2**, the |E/D| value is found to be significantly large and is close to the rhombic limit (|E/D|~0.3), therefore the sign of *D* in complex **2** cannot be predicted unambiguously by calculation. Although single crystal X-ray diffraction studies reveal that all the three complexes possess distorted T_d geometry, in reality they have only C_2v symmetry. Thus, lowering of symmetry allows rigorous mixing between the ground and the excited states, leading to a large zfs in these complexes. The tetrahedral Co(II) ligand field terms are $^4T_2(F)$, $^4T_1(F)$ and $^4T_1(P)$ which further splits in to [($^4A_2$+$^4B_1$+$^4B_2$), ($^4A_1$+$^4B_1$+$^4B_2$) and ($^4A_2$+$^4B_1$+$^4B_2$) states respectively in C_2v symmetry, thus total nine spin-allowed transitions are possible. The computed spin allowed d-d transitions are listed in Tables S8-S11 (also see Figure S9). The d-d transitions belong to the single excitation $^4A_2 \rightarrow {}^4T_2(F)$ and $^4A_2 \rightarrow {}^4T_1(F)$ are found below <10000 cm^{-1} (see table 4 for details) and this explains why the UV-VIS absorption spectrum recorded for all the three complexes did not capture these transitions. On the other hand, the transition which arises from the double excitations $^4A_2 \rightarrow {}^4T_1(P)$ are captured in the UV-vis absorption spectrum. Three distinct peaks are observed for all the three complexes (features of low-symmetry) in the range of 525 to 825 nm (see Figure 9) The d-d transitions computed at CAS (7,5 and 13,8) level of theory are overestimated compared to experiment and this is likely due to the lack of dynamic correlation. However, inclusion of the dynamic correlations using NEVPT2 method yield slightly better results. The calculated absorption spectrum for all complexes **1**-**3** along with experimental observations are provided in the ESI (see Figure S9). Despite the high-level theory employed to reproduce the UV-vis spectra, apparent deviations from experiments are still noted. This is attributed to the fact that the calculations performed includes only selected electrons in the reference space, while this is generally sufficient for magnetic anisotropy, very large reference space including that of ligands are required to reproduce the exact positions of the absorption spectra. This has been witnessed earlier in several mononuclear complexes.[12a, 20] Both experimental and computed d-d transitions show a red shift as we move from –Cl to –I in complexes **1**-**3** and this is essentially due to the fact that, iodide ligand offers smaller crystal field splitting and small inter-electronic repulsion which results into low-lying excited states. For all the complexes **1**-**3**, the ground state wavefunction heavily mixed with other excited states. For complex **1**, the ground state has 48% of $(d_{x^2-y^2})^2$ $(d_{z^2})^2$ $(d_{xy})^1$ $(d_{xz})^1$ $(d_{yz})^1$ composition while 26% of $(d_{x^2-y^2})^1$ $(d_{z^2})^2$ $(d_{xy})^2$ $(d_{xz})^1$ $(d_{yz})^1$ composition.

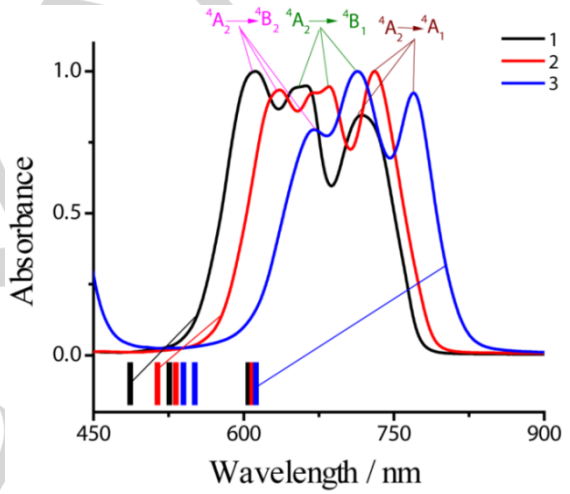

Figure 9. UV-Vis absorption spectroscopy for complexes **1**-**3** were performed in ethylacetate solution in the range of 450-900 nm. Colored sticks represent the computed absorption bands for $^4A_2 \rightarrow {}^4T_1(P)$ transitions with CAS(13,8) level of theory.

The mixing is even more rigorous for –Br and –I analogues (see ESI for details). Not only the single-excitations, but also the states arising from the double excitations are found to be strongly mixed with the ground state wavefunction. This highlights the need for a genuine multi-reference method to compute the spectroscopic properties of these systems.[21] To understand the origin of magnetic anisotropy in these class of complexes, we have first analyzed the state-by-state contributions and then correlated these transitions with the orbital ordering. The state-by-state contribution to the *D* value for all the complexes **1**-**3** is detailed in table 4. From table 4, it is evident that the largest contribution to the *D* value arises from the $^4T_2(F)$ excited state (assuming T_d environment), while other quartet states marginally contribute to *D* value. Among these three transitions, two transitions offer positive contribution to the *D* value, while third transition always contributes to the negative *D* value.

Table 4. CASSCF (7,5)+NEVPT2 computed Spin-Hamiltonian parameter (g, *D*, |E/D|) along with listed state-by-state contribution to the *D* values.

States	1		2		3	
	CASSCF	**NEVPT2**	**CASSCF**	**NEVPT2**	**CASSCF**	**NEVPT2**
	Contribution to D (cm^{-1})		Contribution to D (cm^{-1})		Contribution to D (cm^{-1})	
$^4T_2$(F)	26.46	18.99	27.46	19.03	12.22	7.74
	16.14	10.94	16.64	11.05	12.75	8.09
	-19.52	-13.48	- 25.04	-16.67	-59.81	-40.01
	-2.909	-2.949	-2.747	-2.760	-2.289	-2.277
^{2}G	5.084	5.322	5.409	5.454	4.829	4.853
	1.054	1.089	-1.375	-1.391	-1.848	-1.813
D_{tol}	**21.69**	**17.38**	**18.84**	**14.89**	**-24.68**	**-18.31**
|E/D|	0.26	0.25	0.33	0.31	0.23	0.25
g_{xx}	2.2172	2.1596	2.2663	2.1878	2.2856	2.1941
g_{yy}	2.4125	2.3001	2.4211	2.2983	2.4238	2.2936
g_{zz}	2.5539	2.4101	2.5774	2.4154	2.6644	2.4675

This is due to the different nature of transition dipole moments (*vide infra*). Apart from the quartet $^4T_2$ state, we have also noticed some contribution from the low-lying ^{2}G state; however, it has little effect on the overall zfs parameter. Here, we have provided the splitting pattern of the low-lying excited states for the complex **3** (see figure 10). The observed splitting pattern are in line with the previous studies on the low-symmetric Co(II) complexes. Here, we have analyzed CAS (7,5) orbitals to rationalize these different contributions to the *D* value. The energy ordering of the CAS (7,5) orbitals are in provided in figure 11, which is accordance with ligand field paradigm of the C_{2v} symmetry. The three different excitations corresponding to the $^4T_2$ can be assigned as excitation from the $(d_x^2\text{-}_y^2)^2 \rightarrow t_2$ subshell ($(d_{xy})^1$ $(d_{xz})^1$ $(d_{yz})^1$). The negative contribution to the *D* value is due to spin-conserved excitation between $(d_x^2\text{-}_y^2)^2 \rightarrow (d_{xy})^1$ orbitals as both orbital belong to same $|m_l|$ level. The other two excitations $(d_x^2\text{-}_y^2)^2 \rightarrow (d_{yz})^1/(d_{xz})^1$ leading to a positive zfs contribution (see table 4 for details).[19]

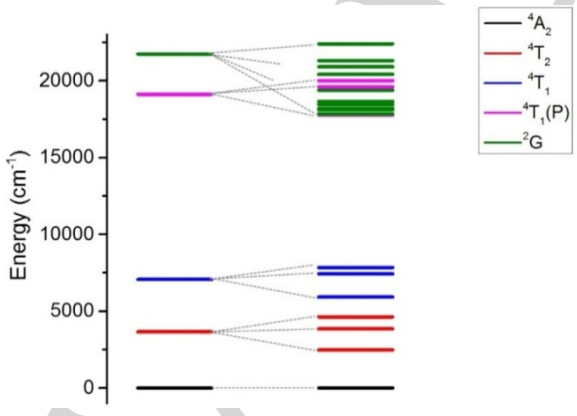

Figure 10. The splitting pattern of the of few low-lying quartet and doublet states ($^4T_2$(F), $^4T_1$(F), $^4T_1$(P) and ^{2}G) for complex **3**.

The small contributions from the low-lying doublet $^2T_2$ (^{2}G) states arises due to the intra singly occupied molecular orbital transitions within t_2-subshell. Inclusion of the dynamic correlations slightly decreases the magnitude of the *D* value; however, the sign of the *D* value remains unchanged. This is due to the fact that the dynamic correlation strongly stabilizes the ground state compared to the excited quartet state, and this led to the increase in the energy gap between the ground and excited quartet state, which eventually decreases the magnitude of the *D* value. On the other hand, doublet states are strongly affected by the dynamic correlation, however, transitions of similar magnitude and opposite sign cancels out each other leading to a negligible contribution to the total *D* value. The orientation of the *D*-tensor for complexes **1**-**3** are provided in the figure 12.

The negative contribution to the *D* value increases as we move down from –Cl to –I, and this might be due to the fact that large spin-orbit coupling constant associated with the heavier halide, brings the excited states closer to the ground state, and hence the increase in the magnitude of the *D* value (see table 4 for details). [22] To cross-check, whether it is an effect of heavier halide or local structural distortion (∠S-Co-S angle 96°(1) and 100°(3)), we have performed additional calculations on a model complex of **3** where –I ligand is substituted by –Cl, without altering the Co-Cl bond distance (named as **3a**). Calculations on model complex **3a** yields a *D* value of +17.4 cm^{-1} and |E/D| value of 0.19, very similar to the complex **1** (see Figure S10 and Figure S11). This clearly highlights that the zfs of Co(II) ion in complexes **1**-**3** are influenced strongly by the presence of heavier ligand like iodide in the first coordination sphere than the local structural distortions.

This is in line with previous observations on pseudo-tetrahedral Co(II) complexes, where the sign of the *D* values is found to be sensitive to the nature of metal-ligand interaction (negative *D* for soft ligands).[12-14] The rhombic zero-field splitting *E* arises due to difference between the D_{XX} and D_{YY} components; the larger the difference, large is the *E* value. The difference in the D_{XX} and D_{YY} components can be rooted back to the different strength of the single-electron excitation from the e-subshell to d_{xz} and d_{yz} orbitals of t_2-subshell. We have observed a significant splitting

between the d_{xz} and d_{yz} orbitals, this eventually led to large difference between the D_{XX} and D_{YY} components; hence the large |E/D| values. The large splitting between the d_{xz} and d_{yz} orbitals are due to the presence of two different donor atoms possessing varying σ/π-donor abilities. The d_{xz} orbital is found to interact with the sulphur, while the d_{yz} orbital interacts with -X ion leading to a large splitting between these two orbitals in all three complexes. On the other hand, the presence of four sulphur atoms would results in a nearly degenerate d_{xz}/d_{yz} orbitals, thus a lower |E/D| values as observed earlier by our group on $[CoS_4]^{2+}$ SMMs.[12c]

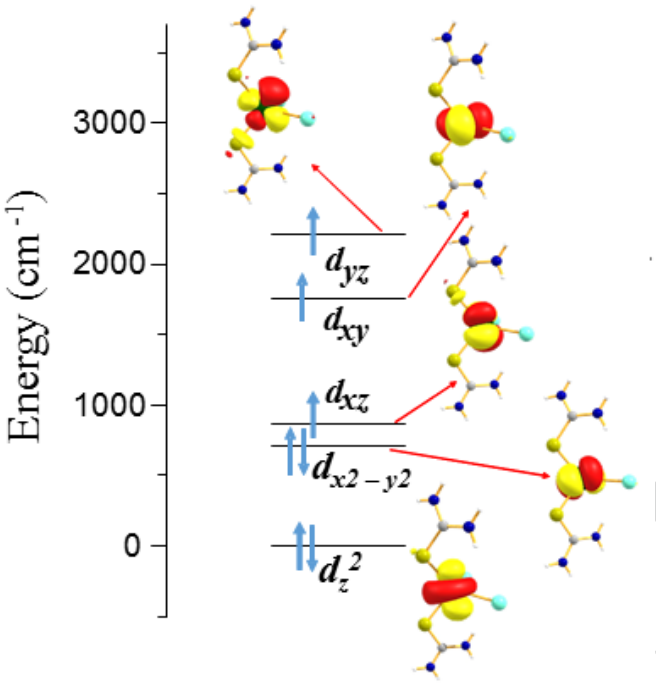

Figure 11. A) CASSCF computed energies of metal based d-orbitals of complex **3**. B) Colour Code. Color Code Co (green); S (light yellow); I (turquoise); N (blue); C(grey) and H (white).

To understand the impact of metal-ligand covalency on the zfs parameter, it is of prime importance to extend the active space by incorporating some ligand orbitals which strongly mix with metal based orbitals, i.e. ligand orbitals with sizable tails on the metal center.

For the tetrahedral Co(II) complexes, here, we have considered the three σ bonding orbitals (d_{xz}+L, d_{yz}+L and d_{xy}+L (where L = ligand orbitals)) in the active space to describe the metal-ligand covalency. Incorporation of these three σ bonding orbitals offers a way to analyze the effect of ligand to metal charge transfer on magnetic anisotropy. One can also incorporate the π-orbitals in active space, however, σ-bonds offers a better picture of metal-ligand covalency as the σ-overlaps are more pronounced that π-overlaps. With an extended active space of CAS(13,8), we have computed all the ten quartets and forty doublets in the configuration interaction module for all the three complexes. The computed *D* (|E/D|) values are found to be +19.2 (0.27) for **1**, ±16.9(0.33) for **2** and -22.4 (0.21) for complex **3** The computed |E/D| values are in line with previous calculations with minimal active space of CAS(7,5) i.e. seven Co(II) based electrons in five Co(II) based orbitals. However, the computed *D* values with CAS(13,8) are marginally (~2-4 cm^{-1}) higher than that computed with the minimal active space of CAS(7,5). Interestingly, the increment in the *D* value is found to be largest for the complex **3** and smallest for the complex **1**. To correlate these changes in the *D* values with the metal-ligand covalency, we have analyzed the eigenvalue plots of complex **1**-**3**. If we look at the figure 13, we notice two important features, (i) splitting of the d-manifold falls in the narrow region as we move towards the heavier halides, (ii) the σ bonding orbitals are much closer in energy to the metal-based d-orbitals for complex **3** followed by complex **2** and **1** (Figure 13).

The first feature is essentially due to the weak ligand field offered by the heavier halides, which results into a smaller crystal field splitting. The second feature highlights the increase in the metal-ligand covalency, where gap between the metal and ligand based orbitals decreases as we move towards the heavier halide. The decrease in the gap between these orbitals led to strong overlap which is directly proportional to the degree of covalency (see the coefficients in figure 13) [23]. Thus, the near degeneracy between the ligand and metal-based orbitals explains the important contribution of the ligand to metal charge transfer excitations in the ground state wavefunction. Not only the *D* value, incorporation of such non-dynamic correlations by extending the active space shows pronounced effect on the absorption spectrum (see Table S11). Furthermore, incorporation of double shell which increases the radial electron correlation may further improvise the obtained spectroscopic properties.[24] Finally, our method suggests that the extended active space calculations offer a clear picture of metal-ligand covalency and its effect on the magnetic anisotropy. Our calculations demonstrate that, presence of large spin-orbit coupling associated with heavier halide is not only the sole factor for increase in the zfs of transition metal complexes, as metal-ligand covalency drastically affects the nature of excitations and thus the zfs. [25]

Magneto-Structural *D*-correlation

To further understand the influence of structural parameters on the sign and magnitude of *D* value in Co(II) tetrahedral complexes, we have developed a magneto-structural correlation on complex **3**. Here, we have systematically varied the ∠S-Co-S and ∠I-Co-I bond angles to generate the tetragonally compressed and elongated structures.[24] In complex **3**, the ∠S-Co-S and ∠I-Co-I bond angles are found to be 100° and 107° respectively, which suggests that complex **3** possess an elongated tetrahedral geometry. Here, we have defined a parameter called δ (δ = $2T_d$-(α+β)) (where T_d represent the angle of 109.5°, while α represents the ∠S-Co-S bond angle while β represents the ∠I-Co-I bond angle) and developed a correlation based on the variation in the δ value. The negative value of δ represents the flattening of tetrahedral geometry while positive value of δ represents tetragonal elongation geometry (see figure 14 for details). It is evident from the figure 14, that with the increase in the δ value, the *D* value increases linearly and for the largest δ value of 50°, the *D* value raised as high as -86 cm^{-1}. Thus, we observed the fourfold increase in the *D* value compared to the parent complex **3** (δ = 11.4).

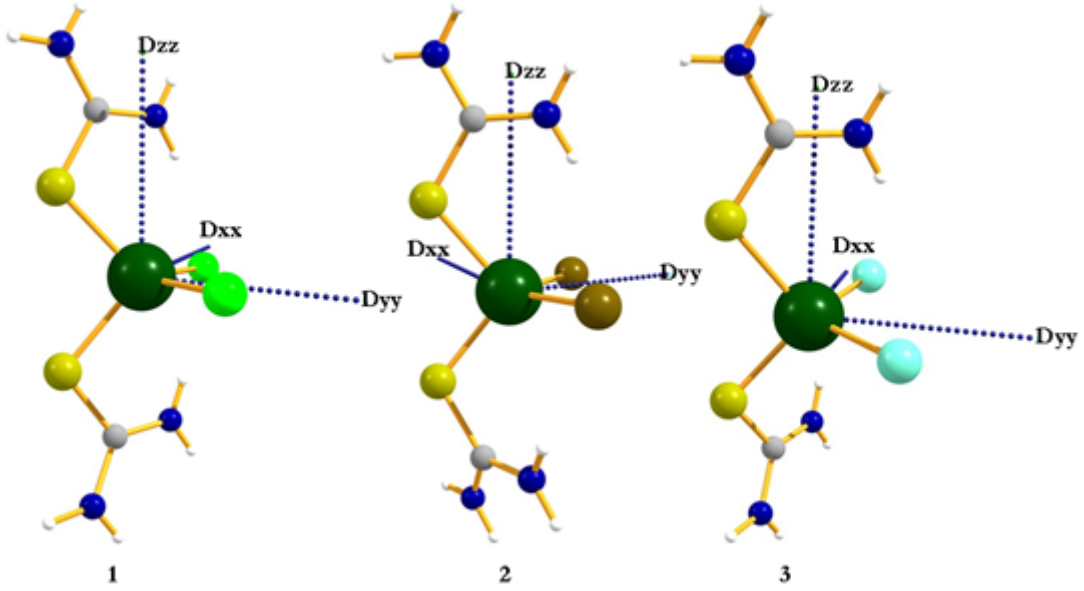

Figure 12. NEVPT2 calculated orientation of the main magnetic axes (*D*-tensor) for complexes A) **1**, B) **2** and C) **3**. Color Code Co (green); S (yellow); Cl (light green);Br (brown); I (turquoise); N (blue); C (grey) and H (white).

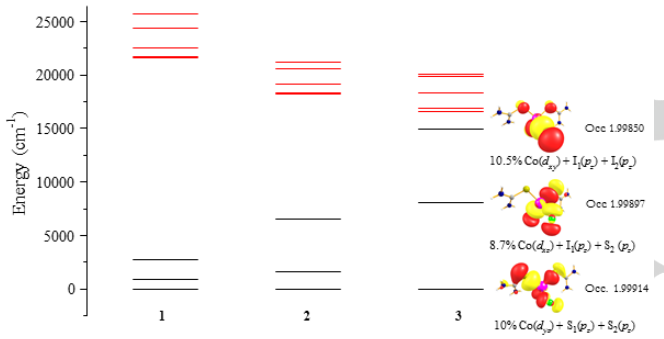

Figure 13. CASSCF computed orbital energies for complex **1-3.** The thick black lines represent the σ-bonding orbital while the red lines represent the *d*-orbital splitting

Besides, the |E/D| value also decreases as the δ increases. Here, we have plotted the variation of the *D* and |E/D| values with change δ value along with variation of the first three excited state E_1, E_2 and E_3 (which belong to the $^4T_2$(F) in T_d symmetry,) and ground state with δ value. The gradual increase in the *D* value with the increase in δ value is due to the lowering of the first excited state (E_1) close to the ground state. However, the other two excited states E_2 and E_3 show an antagonizing behavior, moving away from the ground state, as the δ value increases. The splitting pattern of the first three excited state for the structures corresponding to the large δ values show a typical splitting pattern associated with D_2d symmetry (where $^4A_2$ ground state transforms into $^4B_2$ state and the first excited state $^4T_2$) splits into $^4B_1$ and ^4E state).

The close proximity of the $^4B_1$ state to the $^4B_2$ ground state is the key behind the giant zfs associated with Co(II) complexes in D_2d point group.[12, 26] On the other hand, the non-degenerate nature of second and third excited states (^4E for D_2d symmetry) is due to the asymmetry in the bond angle and difference in the donor strength of ligands. In the other half of the magneto-structural correlations, decrease in the δ value slowly decreases the *D* value at δ value of +3.45 (close to tetrahedron), however, we have not noticed a change in the sign of the *D* value.

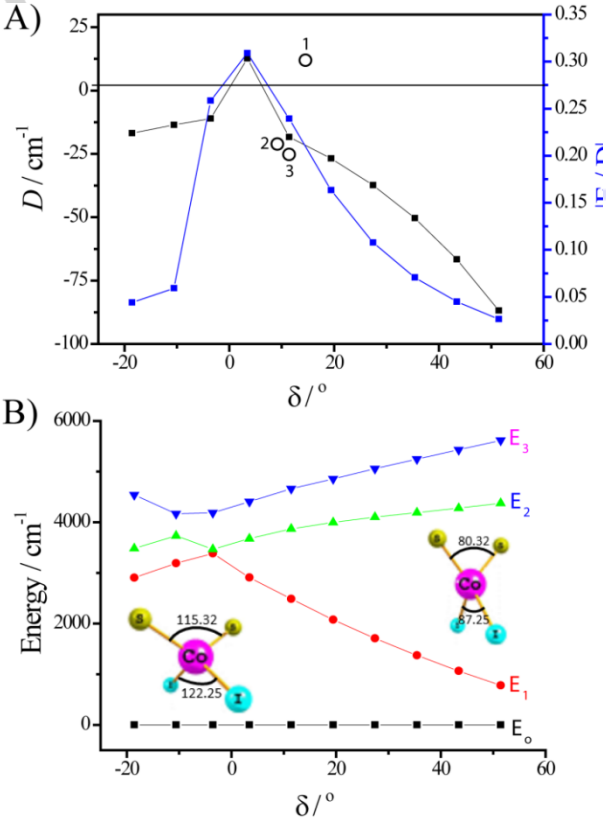

Figure 14. A) Variation of the *D* and |E/D| values with change in the δ value along with the corresponding parameters observed for complexes **1**-**3**; The *D*-value observed for complexes **1**-**3** is mapped (open circle symbol) in the correlation developed based on the δ-value in respective complexes. B) Energy variation of the ground and first three excited states originating from ^4T with respect to the change in the δ value. The graphs constructed here, are based on the values computed at NEVPT2 level of theory. The SH parameters of the complexes **1**-**3** is mapped in left panel.

The sign of *D* cannot be determined unambiguously for this structure as the |E/D| reaches as high as 0.3 at this δ value (+3.45). The decrease in the magnitude of the *D* value can be directly correlated with energy of the first excited state, which becomes higher in the energy for complexes with small δ values. Unlike the scenario observed in tetragonal elongation correlation, the *D*-value does not change abruptly in tetragonal compressed Co(II) geometry. The developed correlations highlight the importance of tetragonal compression and elongation, which directly correlates to the sign, and magnitude of *D*-value of $\{CoL_2X_2\}$ type of complexes.

Finally, to shed the light on SMM characteristic of these complexes, we have first analyzed the wavefunction of the ground state KD for all the complexes. In all the three complexes, the ground state KD are not well isolated, they found to be strongly mixed with other excited state KD. For complex **3**, the ground state KD (represented as $|S,\pm Ms\rangle$) is comprised of 80% $|3/2,\pm3/2\rangle$ and 18% $|3/2,\pm1/2\rangle$ components, which is in principle restricted for a Kramers ion. As for the Kramers ion, these two states must be orthogonal in zero field, and therefore QTM effects are expected. However, the large E term allows the mixing between the ground and excited KDs. This mixing of the state and the apparent splitting of these states by, the large hyperfine spin of the Co(II) triggers the QTM, even in zero field. This could be one of the possible reasons behind the absence of zero field SMM characteristic in the complex **3**. This has been witnessed earlier in other mononuclear Co(II) complexes (see Table S12).[19] Interestingly, for complex **1**, we have observed the out-of-phase signal in the presence of applied magnetic field.[18, 27] To understand this scenario, we have first analyzed decomposition of ground state wavefunction and for complex **1**, the ground state KD is comprised of 70% $|3/2,\pm1/2\rangle$ and 22% $|3/2,\pm3/2\rangle$ Such strong mixing between the ground and excited KD occurs due to the presence of large E/D term (E/D ~ 0.24). In principle, for M_s =1/2, there no preferred easy axis for magnetization in presence of pure axial symmetry. However, presence of large E term ((Dxx-Dyy)/2), creates a preferred easy axis of orientation within the –xy plane. The relaxation enabled via –x(-y) to +x(+y) direction depending on the sign of the E term. However, for the M_s =1/2 as the ground state, the QTM is strong leading to faster relaxation. On the other hand, if one applies the static d.c field, the QTM gets suppressed and a slow relaxation can be observed In literature, there are several examples, where Co(II) complexes show field induced SMM characteristics, even with positive zfs.[19] In such cases, the barrier height can be assigned as $2|E|$ (D_{xx} -D_{yy}) rather than $2|D|$. The computed energy barrier for complex **1** is found to be (~$2|E|$ = 6.09 K), which is good agreement with U_{eff} of complex **1** (U_{eff} = 13.5 and 8.15 K for major and minor relaxation respectively). The presence of field induced SIM characteristic in complex **1**, is due to the presence of positive zfs with remarkably large |E/D| value. Interestingly, the large |E/D| terms offers a key for molecules to show slow relaxation of magnetization with positive *D* values.

Conclusions

To conclude, we have isolated a series of tetrahedral Co(II) complexes with the general molecular formula $[CoL_2X_2]$ (X = Cl (**1**) or Br (**2**) or I (**3**)) which are structurally characterized by the single crystal X-ray diffraction. Direct current magnetic susceptibility measurements performed on the polycrystalline sample of all the complexes indicates the presence of magnetic anisotropy associated with the complexes. The parameters extracted from magnetic data fitting (simultaneous fitting of $\chi_M T(T)$ and $M(H)$) of all the complexes are in excellent agreement with the experimental magnetic data, suggest the reliability of the parameters extracted. The magnetic data fitting evidently shows that complex **1** stabilizes easy plane magnetic anisotropy while **2** and **3** found to possess easy axis magnetic anisotropy. This is qualitatively supported by EPR measurements on these complexes. Alternating current magnetic susceptibly measurements performed on all complexes, but none of the complexes show frequency dependent out-of-phase susceptibility (χ_M'') in the absence of external magnetic field. On the other hand, ac measurements on 10% diluted sample of **1**-**3** apparently show χ_M'' signals in the presence of optimum external magnetic field suggests that the slow relaxation phenomenon is originates from single molecule, which also signifies the influence of dipolar interaction on magnetization relaxation dynamics. The nature of the spin-Hamiltonian parameters extracted and observed magnetization relaxation behavior was rationalized by the electronic structure calculations. Calculations suggests that, the large negative D value for complex **3**, as compared to **1** and **2** is due to the larger metal-ligand covalency of Co-I bond compared to Co-Cl and Co-Br bonds in **1** and **2** respectively. The increase in the metal-ligand covalency has positive impact on the stabilizing easy axes of anisotropy in Co(II) complexes. Also, we rationalize for the absence of slow magnetic relaxation behavior in **1** - **3** is due to the lack of pure ground state in all complexes, further the large |E/D| value triggers the QTM effectively rather thermally assisted Orbach process.[2l, 28] The lack of isolated ground state and the large |E/D| is correlated and routed back to the structural distortion present in all the complexes. In addition, the hyperfine interaction is likely to have non-negligible contribution to the QTM behaviour observed in all the complexes. Overall, the present study reveals that not only, the soft donors such as sulfur modulate the sign and magnitude of *D* (which is the case for some of the recent reports) but also other ligands such as halides holds the key to alter the magnitude and sign of *D*-value of complexes. Further, the study reveals that heavier ligated atoms with large spin-orbit coupling enhances the metal ligand covalency which tend to stabilize easy axis magnetic anisotropy in tetrahedral Co(II) complexes. To generalize further, if a tetrahedral Co(II) ion surrounded by similar π/σ strength soft donor ligand ought to stabilize easy axis anisotropy with small $|E/D|$ ratio is which is an useful finding, particularly for synthetic chemist involved in revealing new generation of single ion magnets.

Experimental Section

All the chemicals were purchased from commercially available sources (Alfa Aesar and Sigma-Aldrich). All the reactions were performed under aerobic conditions. A Perkin-Elmer FT-IR spectrometer (in 400 to 4000 cm^{-1} range) was used to collect the infrared spectra for the polycrystalline samples using KBr pellets. Magnetic susceptibility measurements were performed using a MPMS SQUID magnetometer equipped with 7 Tesla magnet in 300–2.0 K. The single crystal X-ray data were collected in Rigaku-Saturn CCD diffractometer. Details of data collection and structure solution methods were reported elsewhere.[12c] Elemental analysis was carried out on a Thermo Finnigan model. The powder XRD data was collected on a Panalytical MRD System. The absorption profile

for all the complexes were collected on a Jasco V-530 UV/Vis spectrophotometer. Electron paramagnetic resonance spectra were recorded on a broker EMX-plus X-band (9.37 GHz).

Computational Details

All the quantum-chemical calculations were performed on the X-ray structures using ORCA[21b, 29] suite of code. To compute the nature of low-lying excited states and zero-field splitting parameters, we have opted the multi-reference ab initio calculations. State-average complete active space self-consistent field (CASSCF) calculations along with N-electron valence perturbation theory (NEVPT2) were performed on complexes **1**-**3**. NEVPT2 calculations have been performed on top of the converged CASSCF wavefunction to recover the dynamic correlation.[30] Scalar relativistic effects are treated using second-order Douglas-Kroll-Hess (DKH) method.[31] All these procedures were carried out with all electron segmented basis set def2-TZVP for all the atoms. The resolution of identity (RI) approximation has been used with the corresponding auxiliary basis sets in order to speed up the calculations.[32] Two set of calculations have been performed, where we have chosen two different active spaces. The first active space is the minimal active space which comprised of seven active d-electron in the five Co(II) based d-orbitals (CAS(7,5)). Here, we have computed all the 10 quartet and 40 doublet states. To understand the effect of the ligands, especially the nature of metal-ligand covalency, we have extended an active space by incorporating three σ bonding orbitals in the active space. Hence, the new active space comprises CAS(13,8); 6 electrons of the 3 σ bonding orbitals along with seven d-electrons in the five active Co(II) based d-orbitals. The 10 quartet and 40 doublets are computed with CAS(13,8) active space. Apart from computing the Spin-Hamiltonian parameters, we have also done survey for the fitting of magnetization and susceptibility data to check the quality of fit.

Synthetic procedure for the isolation of complexes 1-3

Complex $[Co(L)_2Cl_2]$ (**1**)

To warm (35-40°C) ethanol, solid $CoCl_2.6H_2O$ (1.55g, 6.5 mmol) was added. Into this solution L (1g, 13.2 mmol) was added and the reaction mixture was heated under reflux for 12 hours. The ethanol solvent was removed under reduced pressure (roto vap) after cooling the reaction mixture. The complex of interest was extracted from acetonitrile. Needle shaped blue colour single crystals were grown from filtrate by diffusion of diethylether into acetonitrile solution after one week at room temperature. Yield: 1.2 g (32.4%) Elemental analysis: Calc: C, 8.5%; H, 2.8%; N, 19.8%; S, 22.7% Found: C, 8.42%; H, 2.3%; N, 19.6%; S, 22.1%. IR (KBr): 3329 and 3391 cm^{-1} (ν_{NH2}) and 1620 cm^{-1} ($\nu_{C=S}$).

Complex $[Co(L)_2Br_2]$ (**2**)

A similar synthetic procedure was followed as in **1**, $CoBr_2$ (1.43g, 0.0065 mol) was used in place of $CoCl_2.6H_2O$. Further, the product of interest was extracted from ethylacetate rather than acetonitrile. Unlike in **1**, single crystals were obtained by slow evaporation of ethylacetate solution. X-ray quality blue colour single crystals were grown from filtrate within a week at room temperature. Yield: 1.7g (35.4%) Calc: C, 6.5%; H, 2.17%; N, 15.1%; S, 17.3% Found: C, 6.38%; H, 2.5%; N, 14.84%; S, 17.5%. IR (KBr):- 3313 and 3391 cm^{-1} (ν_{NH2}) and 1634 cm^{-1} ($\nu_{C=S}$).

Complex $[Co(L)_2I_2]$ (**3**)

A similar synthetic procedure was followed as in **2**, CoI_2 (2.05g, 0.0065 mol) was used in place of $CoBr_2$. Yield 0.7g (11.4%). Calc: C, 5.2%; H, 1.7%; N, 12.1%; S, 13.8% Found: C, 5.16%; H, 2.1%; N, 11.75%; S, 13.1%. IR (KBr):- 3300 and 3417 cm^{-1} (ν_{NH2}) and 1606 cm^{-1} ($\nu_{C=S}$).

The bulk samples phase purity (complexes **1**-**3**) was confirmed by powder x-ray diffraction. The experimental data is in well agreement with simulated data (see Figure S12).

Complex $[Zn(L)_2Cl_2]$ (**1-Zn**)

Similar synthetic procedure was followed as for **1**, $ZnCl_2$ (0.895g, 6.57 mmol) was used in place of $CoCl_2.6H_2O$. Yield 0.9g (42.4%). Calc: C, 8.33%; H, 2.79%; N, 19.42%; S, 22.23% Found: C, 8.5%; H, 2.6%; N, 19.3%; S, 22.4%. IR (KBr):- 3312 and 3386 cm^{-1} (ν_{NH2}) and 1591 cm^{-1} ($\nu_{C=S}$).

Complex $[Zn(L)_2Br_2]$ (**2-Zn**)

Similar synthetic procedure was followed as for **2**, $ZnBr_2$ (1.48g, 6.57 mmol) was used in place of $CoBr_2$. Yield 0.59g (34.7%). Calc: C, 6.36%; H, 2.14%; N, 14.7%; S, 17.2% Found: C, 6.3%; H, 2.22%; N, 14.7%; S, 17.2%. IR (KBr):- 3342 and 3401 cm^{-1} (ν_{NH2}) and 1618 cm^{-1} ($\nu_{C=S}$).

Complex $[Zn(L)_2I_2]$ (**3-Zn**)

Similar synthetic procedure was followed as for **3**, ZnI_2 (2.1g, 6.57 mmol) was used in place of CoI_2. Yield 0.62g (41%). Calc: C, 5.10%; H, 1.71%; N, 11.88%; S, 13.6% Found: C, 5.17%; H, 1.65%; N, 11.96%; S, 13.42%. IR (KBr):- 3285 and 3362 cm^{-1} (ν_{NH2}) and 1584 cm^{-1} ($\nu_{C=S}$).

The unit cell was checked for the single crystals obtained for **1-Zn**, **2-Zn** and **3-Zn** and the unit cell of all the complexes is in excellent agreement with unit cell of the corresponding parent Co(II) complexes. This implies that **1-Zn**, **2-Zn** and **3-Zn** possess similar packing diagram of **1**, **2** and **3** respectively. To further give concrete evidence, we have recorded powder x-ray diffraction pattern for **1-Zn**, **2-Zn** and **3-Zn** which is in excellent agreement with the simulated data derived from their parent Co(II) single crystal data. (see Figure S13).

Preparation of 10% diluted sample of **1**.

To warm (35-40°C) ethanol, solid $CoCl_2.6H_2O$ (0.156g, 0.657 mmol) and $ZnCl_2$ (0.807g, 5.92 mmol) was added. Into this solution L (1g, 13.2 mmol) was added and the reaction mixture was heated under reflux for 12 hours. The ethanol solvent was removed under reduced pressure (roto vap) after cooling the reaction mixture. The complex of interest was extracted from acetonitrile. Needle shaped light blue single crystals were grown from filtrate by diffusion of diethylether into acetonitrile solution after one week at room temperature.

Preparation of 10% diluted sample of **2**.

To warm (35-40°C) ethanol, solid $CoBr_2$ (0.144g, 0.657 mmol) and $ZnBr_2$ (0.666 g, 5.92 mmol) was added. Into this solution L (1g, 13.2 mmol) was added and the reaction mixture was heated under reflux for 12 hours. Further, the product of interest was extracted from ethylacetate rather than acetonitrile. Light blue single crystals were obtained by slow evaporation of ethylacetate solution.

Preparation of 10% diluted sample of **3**.

To warm (35-40°C) ethanol, solid CoI_2 (0.206g, 0.657 mmol) and ZnI_2 (1.88g, 5.92 mmol) was added. Into this solution L (1g, 13.2 mmol) was added and the reaction mixture was heated under reflux for 12 hours. Further, the product of interest was extracted from ethylacetate rather than acetonitrile. Light blue single crystals were obtained by slow evaporation of ethylacetate solution.

CCDC numbers: 1504900-1504902.

Acknowledgements

M.S. thanks the funding agencies DST, DST Nanomission, INSA, and IIT Bombay for financial support. S.V. and P.S. thanks CSIR for financial support. K.A. thanks UGC for financial support.

Keywords: Single ion magnet (SIM) • Cobalt(II) • ab initio calculation • magneto structural correlation

References

[1] a) R. Sessoli, D. Gatteschi, A. Caneschi, M. A. Novak, **1993**, *365*, 141-143; b) A. Caneschi, D. Gatteschi, R. Sessoli, A. L. Barra, L. C. Brunel, M. Guillot, *J. Am. Chem. Soc.* **1991**, *113*, 5873-5874.
[2] a) A. Nava, L. Rigamonti, E. Zangrando, R. Sessoli, W. Wernsdorfer, A. Cornia, *Angew. Chem., Int. Ed.* **2015**, *54*, 8777-8782; b) M. Ako Ayuk, V. Mereacre, Y. Lan, W. Wernsdorfer, R. Clerac, E. Anson Christopher, K. Powell Annie, *Inorg Chem* **2010**, *49*, 1-3; c) R. Pattacini, P. Teo, J. Zhang, Y. Lan, K. Powell Annie, J. Nehrkorn, O. Waldmann, T. S. A. Hor, P. Braunstein, *Dalton Trans* **2011**, *40*, 10526-10534; d) M. Ibrahim, Y. Lan, S. Bassil Bassem, Y. Xiang, A. Suchopar, K. Powell Annie, U. Kortz, *Angew Chem Int Ed Engl* **2011**, *50*, 4708-4711; e) Y.-Z. Zhang, A. J. Brown, Y.-S. Meng, H.-L. Sun, S. Gao, *Dalton Trans.* **2015**, *44*, 2865-2870; f) Y.-Y. Zhu, C. Cui, K. Qian, J. Yin, B.-W. Wang, Z.-M. Wang, S. Gao, *Dalton Trans.* **2014**, *43*, 11897-11907; g) C.-L. Zhou, Z.-M. Wang, B.-W. Wang, S. Gao, *Polyhedron* **2011**, *30*, 3279-3283; h)Y.-Y. Zhu, X. Guo, C. Cui, B.-W. Wang, Z.-M. Wang, S. Gao, *Chem. Commun.* **2011**, *47*, 8049-8051; i)A. Perivolaris, A. M. Fidelli, R. Inglis, V. G. Kessler, A. M. Z. Slawin, E. K. Brechin, G. S. Papaefstathiou, *J. Coord. Chem.* **2014**, *67*, 3972-3986; j) S. M. Taylor, J. M. Frost, R. McLellan, R. D. McIntosh, E. K. Brechin, S. J. Dalgarno, *Cryst. Eng. Comm.* **2014**, *16*, 8098-8101; k) J. Martinez-Lillo, N. Dolan, E. K. Brechin, *Dalton Trans.* **2013**, *42*, 12824-12827; l) Y.-Z. Zhang, S. Gomez-Coca, A. J. Brown, M. R. Saber, X. Zhang, K. R. Dunbar, *Chem. Sci.* **2016**, *7*, 6519-6527; m) S. K. Langley, R. A. Stott, N. F. Chilton, B. Moubaraki, K. S. Murray, *Chem. Commun.* **2011**, *47*, 6281-6283; n) S.-S. Bao, L.-M. Zheng, *Coord. Chem. Rev.* **2016**, *319*, 63-85; o) T. K. Prasad, G. Poneti, L. Sorace, M. J. Rodriguez-Douton, A.-L. Barra, P. Neugebauer, L. Costantino, R. Sessoli, A. Cornia, *Dalton Trans.* **2012**, *41*, 8368-8378; p) M. Murrie, *Chem. Soc. Rev.* **2010**, *39*, 1986-1995; q) Y.-Y. Zhu, Y.-Q. Zhang, T.-T. Yin, C. Gao, B.-W. Wang, S. Gao, *Inorg. Chem.* **2015**, *54*, 5475-5486.
[3] A. M. Ako, I. J. Hewitt, V. Mereacre, R. Clerac, W. Wernsdorfer, C. E. Anson, A. K. Powell, *Angew. Chem., Int. Ed.* **2006**, *45*, 4926-4929.
[4] C. J. Milios, R. Inglis, A. Vinslava, R. Bagai, W. Wernsdorfer, S. Parsons, S. P. Perlepes, G. Christou, E. K. Brechin, *J. Am. Chem. Soc.* **2007**, *129*, 12505-12511.
[5] a) M. N. Leuenberger, D. Loss, *Nature* **2001**, *410*, 789-793; b) J. Lehmann, A. Gaita-Arino, E. Coronado, D. Loss, *Nat. Nanotechnol.* **2007**, *2*, 312-317; c) L. Bogani, W. Wernsdorfer, *Nat. Mater.* **2008**, *7*, 179-186; d) R. Sessoli, M.-E. Boulon, A. Caneschi, M. Mannini, L. Poggini, F. Wilhelm, A. Rogalev, *Nat. Phys.* **2015**, *11*, 69-74.
[6] F. Neese, D. A. Pantazis, *Faraday Discuss.* **2011**, *148*, 229-238.
[7] a) D. E. Freedman, W. H. Harman, T. D. Harris, G. J. Long, C. J. Chang, J. R. Long, *J. Am. Chem. Soc.* **2010**, *132*, 1224-1225; b) R. Ruamps, R. Maurice, L. Batchelor, M. Boggio-Pasqua, R. Guillot, A. L. Barra, J. Liu, E.-E. Bendeif, S. Pillet, S. Hill, T. Mallah, N. Guihery, *J. Am. Chem. Soc.* **2013**, *135*, 3017-3026; c) S. Gomez-Coca, D. Aravena, R. Morales, E. Ruiz, *Coord. Chem. Rev.* **2015**, *289-290*, 379-392; d) A. K. Bar, C. Pichon, J.-P. Sutter, *Coord. Chem. Rev.* **2016**, *308*, 346-380; e) G. A. Craig, M. Murrie, *Chem. Soc. Rev.* **2015**, *44*, 2135-2147; f) J. M. Zadrozny, M. Atanasov, A. M. Bryan, C.-Y. Lin, B. D. Rekken, P. P. Power, F. Neese, J. R. Long, *Chem. Sci.* **2013**, *4*, 125-138; g) R. C. Poulten, M. J. Page, A. G. Algarra, J. J. Le Roy, I. Lopez, E. Carter, A. Llobet, S. A. Macgregor, M. F. Mahon, D. M. Murphy, M. Murugesu, M. K. Whittlesey, *J. Am. Chem. Soc.* **2013**, *135*, 13640-13643; h) P. P. Samuel, K. C. Mondal, N. Amin Sk, H. W. Roesky, E. Carl, R. Neufeld, D. Stalke, S. Demeshko, F. Meyer, L. Ungur, L. F. Chibotaru, J. Christian, V. Ramachandran, J. van Tol, N. S. Dalal, *J. Am. Chem. Soc.* **2014**, *136*, 11964-11971; i) C. G. Werncke, E. Suturina, P. C. Bunting, L. Vendier, J. R. Long, M. Atanasov, F. Neese, S. Sabo-Etienne, S. Bontemps, *Chem. - Eur. J.* **2016**, *22*, 1668-1674; j) Y.-S. Meng, Z. Mo, B.-W. Wang, Y.-Q. Zhang, L. Deng, S. Gao, *Chem. Sci.* **2015**, *6*, 7156-7162.
[8] a) J. M. Zadrozny, D. J. Xiao, M. Atanasov, G. J. Long, F. Grandjean, F. Neese, J. R. Long, *Nat. Chem.* **2013**, *5*, 577-581; b) X.-N. Yao, J.-Z. Du, Y.-Q. Zhang, X.-B. Leng, M.-W. Yang, S.-D. Jiang, Z.-X. Wang, Z.-W. Ouyang, L. Deng, B.-W. Wang, S. Gao, *J. Am. Chem. Soc.* **2017**, *139*, 373-380.
[9] a) C. Rajnak, J. Titis, I. Salitros, R. Boca, O. Fuhr, M. Ruben, *Polyhedron* **2013**, *65*, 122-128; b) D. Wu, X. Zhang, P. Huang, W. Huang, M. Ruan, Z. W. Ouyang, *Inorg. Chem.* **2013**, *52*, 10976-10982.
[10] a) F. Habib, O. R. Luca, V. Vieru, M. Shiddiq, I. Korobkov, S. I. Gorelsky, M. K. Takase, L. F. Chibotaru, S. Hill, R. H. Crabtree, M. Murugesu, *Angew. Chem., Int. Ed.* **2013**, *52*, 11290-11293; b) T. Jurca, A. Farghal, P.-H. Lin, I. Korobkov, M. Murugesu, D. S. Richeson, *J. Am. Chem. Soc.* **2011**, *133*, 15814-15817; c) D. Schweinfurth, M. G. Sommer, M. Atanasov, S. Demeshko, S. Hohloch, F. Meyer, F. Neese, B. Sarkar, *J. Am. Chem. Soc.* **2015**, *137*, 1993-2005; d) R. Ruamps, L. J. Batchelor, R. Guillot, G. Zakhia, A.-L. Barra, W. Wernsdorfer, N. Guihery, T. Mallah, *Chem. Sci.* **2014**, *5*, 3418-3424; e) T. J. Woods, M. F. Ballesteros-Rivas, S. Gomez-Coca, E. Ruiz, K. R. Dunbar, *J. Am. Chem. Soc.* **2016**, *138*, 16407-16416.
[11] a) F. Yang, Q. Zhou, Y. Zhang, G. Zeng, G. Li, Z. Shi, B. Wang, S. Feng, *Chem. Commun.* **2013**, *49*, 5289-5291; b) M. Idesicova, J. Titis, J. Krzystek, R. Boca, *Inorg. Chem.* **2013**, *52*, 9409-9417; c) L. Smolko, J. Cernak, M. Dusek, J. Titis, R. Boca, *New J. Chem.* **2016**, *40*, 6593-6598; d) L. Smolko, J. Cernak, J. Kuchar, R. Boca, *Monatsh. Chem.* **2015**, *146*, 243-248; e) F. Habib, I. Korobkov, M. Murugesu, *Dalton Trans.* **2015**, *44*, 6368-6373; f) E. Colacio, J. Ruiz, E. Ruiz, E. Cremades, J. Krzystek, S. Carretta, J. Cano, T. Guidi, W. Wernsdorfer, E. K. Brechin, *Angew. Chem., Int. Ed.* **2013**, *52*, 9130-9134; g) Y.-Y. Zhu, C. Cui, Y.-Q. Zhang, J.-H. Jia, X. Guo, C. Gao, K. Qian, S.-D. Jiang, B.-W. Wang, Z.-M. Wang, S. Gao, *Chem. Sci.* **2013**, *4*, 1802-1806; h) S. Sottini, G. Poneti, S. Ciattini, N. Levesanos, E. Ferentinos, J. Krzystek, L. Sorace, P. Kyritsis, *Inorg. Chem.* **2016**, *55*, 9537-9548; i) S. Ziegenbalg, D. Hornig, H. Goerls, W. Plass, *Inorg. Chem.* **2016**, *55*, 4047-4058.
[12] a) E. A. Suturina, D. Maganas, E. Bill, M. Atanasov, F. Neese, *Inorg. Chem.* **2015**, *54*, 9948-9961; b) D. Maganas, S. Sottini, P. Kyritsis, E. J. J. Groenen, F. Neese, *Inorg. Chem.* **2011**, *50*, 8741-8754; c) S. Vaidya, S. Tewary, S. K. Singh, S. K. Langley, K. S. Murray, Y. Lan, W. Wernsdorfer, G. Rajaraman, M. Shanmugam, *Inorg. Chem.* **2016**, *55*, 9564-9578.
[13] a) S. Vaidya, A. Upadhyay, S. K. Singh, T. Gupta, S. Tewary, S. K. Langley, J. P. S. Walsh, K. S. Murray, G. Rajaraman, M. Shanmugam, *Chem. Commun.* **2015**, *51*, 3739-3742; b) J. M. Zadrozny, J. Telser, J. R. Long, *Polyhedron* **2013**, *64*, 209-217.
[14] J. M. Zadrozny, J. R. Long, *J. Am. Chem. Soc.* **2011**, *133*, 20732-20734.
[15] N. F. Chilton, R. P. Anderson, L. D. Turner, A. Soncini, K. S. Murray, *J. Comput. Chem.* **2013**, *34*, 1164-1175.
[16] a) M. Dey, S. Dutta, B. Sarma, R. C. Deka, N. Gogoi, *Chem. Commun.* **2016**, *52*, 753-756; b) A. Eichhoefer, Y. Lan, V. Mereacre, T. Bodenstein, F. Weigend, *Inorg. Chem.* **2014**, *53*, 1962-1974; c) D. V. Korchagin, G. V. Shilov, S. M. Aldoshin, R. B. Morgunov, A. D. Talantsev, E. A. Yureva, *Polyhedron* **2015**, *102*, 147-151.
[17] a) V. V. Novikov, A. A. Pavlov, A. S. Belov, A. V. Vologzhanina, A. Savitsky, Y. Z. Voloshin, *J. Phys. Chem. Lett.* **2014**, *5*, 3799-3803; b) J. Pilbrow, *Transition Ion Electron Paramagnetic Resonance,Clarendon Press Clarendon Press: Oxford, U.K.* **1990**.
[18] a) J. M. Zadrozny, J. Liu, N. A. Piro, C. J. Chang, S. Hill, J. R. Long, *Chem. Commun.* **2012**, *48*, 3927-3929; b) S. Gomez-Coca, E. Cremades, N. Aliaga-Alcalde, E. Ruiz, *J. Am. Chem. Soc.* **2013**, *135*, 7010-7018; c) W. Huang, T. Liu, D. Wu, J. Cheng, Z. W. Ouyang, C. Duan, *Dalton Trans.* **2013**, *42*, 15326-15331.
[19] S. Gomez-Coca, A. Urtizberea, E. Cremades, P. J. Alonso, A. Camon, E. Ruiz, F. Luis, *Nat. Commun.* **2014**, *5*, 4300.
[20] E. A. Suturina, J. Nehrkorn, J. M. Zadrozny, J. Liu, M. Atanasov, T. Weyhermueller, D. Maganas, S. Hill, A. Schnegg, E. Bill, J. R. Long, F. Neese, *Inorg. Chem.* **2017**, *56*, 3102-3118.
[21] a) D. Ganyushin, F. Neese, *J. Chem. Phys.* **2006**, *125*, 024103/024101-024103/024111; b) F. Neese, T. Petrenko, D. Ganyushin, G. Olbrich, *Coord. Chem. Rev.* **2007**, *251*, 288-327.
[22] S. Ye, F. Neese, *J. Chem. Theory Comput.* **2012**, *8*, 2344-2351.
[23] T. Cundari, *Ed. Computational Organometallic Chemistry; Marcel Dekker, Inc., New York* **2001**.
[24] R. Maurice, R. Bastardis, C. de Graaf, N. Suaud, T. Mallah, N. Guihery, *J. Chem. Theory Comput.* **2009**, *5*, 2977-2984.
[25] S. K. Singh, J. Eng, M. Atanasov, F. Neese, *Coord. Chem. Rev.* **2017**, 10.1016/j.ccr.2017.1003.1018.
[26] Y. Rechkemmer, F. D. Breitgoff, M. van der Meer, M. Atanasov, M. Hakl, M. Orlita, P. Neugebauer, F. Neese, B. Sarkar, J. van Slageren, *Nat. Commun* **2016**, 7, 10467.
[27] J. Vallejo, I. Castro, R. Ruiz-Garcia, J. Cano, M. Julve, F. Lloret, G. De Munno, W. Wernsdorfer, E. Pardo, *J. Am. Chem. Soc.* **2012**, *134*, 15704-15707.
[28] a) V. V. Novikov, A. A. Pavlov, Y. V. Nelyubina, M.-E. Boulon, O. A. Varzatskii, Y. Z. Voloshin, R. E. P. Winpenny, *J. Am. Chem. Soc.* **2015**, *137*, 9792-9795; b) L. Smolko, J. Cernak, M. Dusek, J. Miklovic, J. Titis, R. Boca, *Dalton Trans* **2015**, *44*, 17565-17571.
[29] F. Neese, *Wiley Interdiscip. Rev. Comput. Mol. Sci.* **2012**, *2*, 73-78.
[30] a) C. Angeli, R. Cimiraglia, S. Evangelisti, T. Leininger, J. P. Malrieu, *J. Chem. Phys.* **2001**, *114*, 10252-10264; b) C. Angeli, R. Cimiraglia, J.-P. Malrieu, *Chem. Phys. Lett.* **2001**, *350*, 297-305.
[31] B. A. Hess, *Phys. Rev. A Gen. Phys.* **1986**, *33*, 3742-3748.
[32] F. Neese, *J. Comput. Chem.* **2003**, *24*, 1740-1747.

10.1002/chem.201606031

WILEY-VCH

FULL PAPER

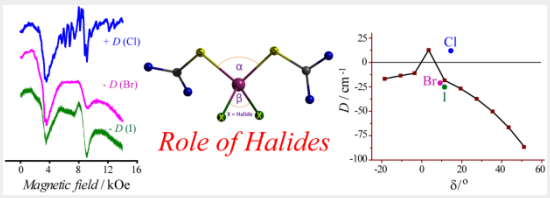

We report a family of tetrahedral Co(II) single-ion magnets with general molecular formula of $[Co(L_1)_2X_2]$ where L_1 = thiourea and X = Cl (**1**), Br (**2**) and I (**3**). Effect of halide ion in modulating the sign as well as magnitude of D in these complexes been studied in detail and the observed experimental results firmly supported by theoretical calculations.

Shefali Vaidya,Saurabh Kumar Singh, Pragya Shukla, Kamaluddin Ansari, Gopalan Rajaraman and Maheswaran Shanmugam**

Page No. – Page No.

Role of Halide Ions on the Nature of Magnetic Anisotropy in Tetrahedral Co(II) Complexes